Thermoelectrical Tick Removal Process Modeling

Nikola Kosturski, Ivan Lirkov, Svetozar Margenov, and Yavor Vutov

Institute of Information and Communication Technologies,
Bulgarian Academy of Sciences, Acad. G. Bonchev, Bl. 25A, 1113 Sofia, Bulgaria

Abstract. Ticks are widespread ectoparasites. They feed on blood of animals like birds and mammals, including humans. They are carriers and transmitters of pathogens, which cause many diseases, including *tick-borne meningoencephalitis*, *lyme borreliosis*, *typhus* to name few. The best way to prevent infection is to remove the ticks from the host as soon as possible. The removal usually is performed mechanically by pulling the tick. This however is a risky process. Tick irritation or injury may result in it vomiting infective fluids.

On a quest of creating of a portable device, which utilizes radio-frequency alternating current for contact-less tick removal, we simulate the thermo-electrical processes of the device application. We use the finite element method, to obtain both the current density inside the host and the tick, and the created temperature field. The computational domain consists of the host's skin, the tick, the electrodes, and air.

Experiments on nested grids are performed to ensure numerical correctness of the obtained solutions. Various electrode configurations are investigated. The goal is to find suitable working parameters – applied power, duration, position for the procedure.

1 Introduction

We are on a quest of developing a contact-less tick removal apparatus. Ticks spread a wide variety of diseases and their removal without disturbance is of a great importance. Ticks are not to be disturbed, because they could vomit potentially contaminated fluids into their host.

The apparatus under development consists of two electrodes. They are applied to the skin of the host, in the vicinity of the tick bite. Then radio-frequency alternating current is started through the electrodes. It is expected that weak electro and thermal stimulation can discomfort the tick and make it leave the host.

The rest of the paper is organized as follows: In Section 1 the model and its mathematical treatment are presented. The setup and the results of the performed numerical experiments are presented in Section 2. Some discussion and concluding remarks are given at the end.

2 The Model, Space, and Time Discretization

We consider the bio-heat equation in the following form [1]:

$$\rho c \frac{\partial T}{\partial t} = \nabla \cdot k \nabla T + J \cdot E \tag{1}$$

where the thermal energy arising from the current flow is described by $J \cdot E$. Here, a simplified model is considered, where metabolic heat production, and air convection effects are ignored. The initial and boundary conditions which are used in this approach are as follows:

$$T = 37^{\circ}\mathrm{C} \qquad \text{when } t = 0 \text{ at } \Omega_{skin} \cup \Omega_{tick} \cup \Omega_{tick\,mouth} \tag{2a}$$

$$T = 20^{\circ}\mathrm{C} \qquad \text{when } t = 0 \text{ at } \Omega_{air} \cup \Omega_{El1} \cup \Omega_{El2}, \tag{2b}$$

$$T = 37^{\circ}\mathrm{C} \qquad \text{when } t \geq 0 \text{ at } \Gamma_{bottom}, \tag{2c}$$

$$T = 20^{\circ}\mathrm{C} \qquad \text{when } t \geq 0 \text{ at } \Gamma_{top}, \tag{2d}$$

$$k \nabla T \cdot \mathbf{n} = 0 \qquad \text{when } t > 0 \text{ at } \Gamma_{side}. \tag{2e}$$

The notations which are used in (1) and (2) are given below:

- Ω – the entire domain of the model;
- $\Omega_{El1}, \Omega_{El2}$ – the domains of the two electrodes;
- $\Omega_{tick}, \Omega_{tick\,mouth}$ – the domains of the body and mouth of the tick;
- $\Omega_{skin} = \Omega_{gel} \cup \Omega_{epidermis} \cup \Omega_{dermis} \cup \Omega_{subcutis}$ – the domains of various skin tissues and the applied electroconducting gel;
- Γ_{top} – the top boundary of Ω_{air};
- Γ_{bottom} – the bottom boundary of Ω_{skin};
- Γ_{side} – The boundary on the side of Ω;
- ρ – density [kg/m^3];
- c – specific heat [J/kg K];
- k – thermal conductivity [W/m K];
- J – current density [A/m];
- E – electric field intensity [V/m];
- t – time [s];
- T – temperature [°C];
- $\mathbf{n}$ – outward facing normal to the boundary.

The computational domain Ω is sketched on Fig. 1. It consists of air, two steel electrodes, electro-conducting gel, and several skin layers – epidermis, dermis, and subcutis. Both tick's mouth and body are present in the domain. The goal is not to model the exact tick geometry, but rather to have a distinct domain in the geometry (especially for the tick mouth) so we can analyze the temperature field there. The outermost epidermis layer – stratum corneum has high electrical impedance, which also varies a lot. To overcome this, we apply electro-conductive gel on top of the skin. In the presented algorithm the bio-heat problem (1) is solved in two steps (see [6] for more details):

1. Finding a steady state heat source $J \cdot E$ using that: (a) $E = -\nabla V$ (V is the electric potential in the computational domain Ω), and (b) $J = \sigma E$, where σ is the electric conductivity [S/m];

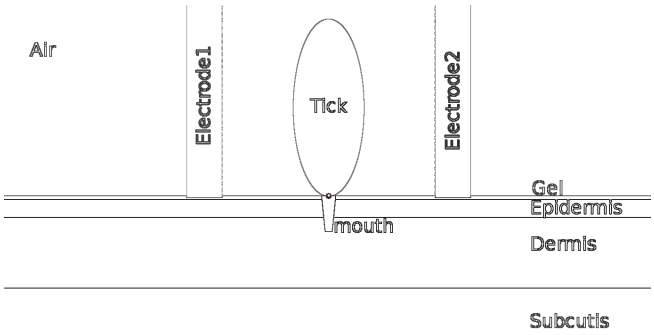

Fig. 1. Computational geometry

2. Finding the temperature T by solving the heat transfer equation (1) using the heat source $J \cdot E$ obtained in the first step.

At first step, in order to determine the heat source $J \cdot E$, we have to find the distribution of the electric potential V. It is known that we can neglect the contribution from the magnetic field in Maxwell's equation if the size of the computational domain is much smaller than the wavelength. We use computer simulation of the electromagnetic processes in a model domain which is a 5 cm $\times$ 5 cm $\times$ 5 cm cube for the electric current with frequency up to 900 kHz. Comsol Multiphysics module "AC/DC module — Electric and induction currents" (see [11]) is applied to solve the Maxwell's equation in the time-harmonic case. The numerical results show that the dependency of the distribution of the electric potential V on the magnetic field is unseen. Thus, the distribution of the electric potential V is found by solving the Poisson's equation:

$$\nabla \cdot \sigma \nabla V = 0, \text{ in } \Omega, \tag{3}$$

with boundary conditions

$$\nabla V \cdot \mathbf{n} = 0 \text{ at } \partial\Omega \setminus \partial\Omega_{El1} \setminus \partial\Omega_{El2}, \tag{4a}$$

$$V = 0 \text{ at } \partial\Omega_{El1} \cap \partial\Omega, \tag{4b}$$

$$V = V_0 \text{ at } \partial\Omega_{El2} \cap \partial\Omega. \tag{4c}$$

The following notations are used in the above equations:

- V – Electric potential in Ω;
- σ – electric conductivity [S/m];
- V_0 – applied voltage;
- $\partial\Omega_{El1}$ – boundary of electrode 1;
- $\partial\Omega_{El2}$ – boundary of electrode 2;
- $\partial\Omega \setminus \partial\Omega_{El1} \setminus \partial\Omega_{El2}$ – the rest of the domain surface.

After determining the potential distribution, the electric field intensity and the current density is computed from

$$E = -\nabla V, \qquad J = \sigma E.$$

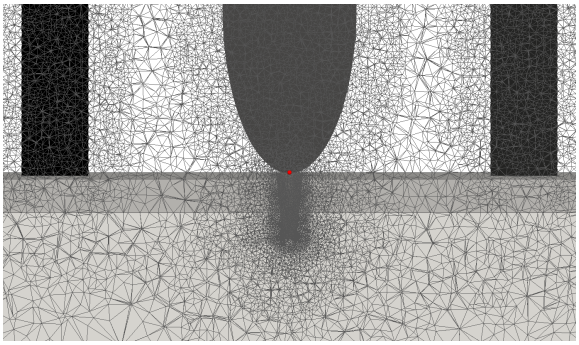

Fig. 2. Computational coarse mesh.

It is more useful to have the output power as an input parameter, than the actual voltage. We have to find the potential V_0 for the last boundary condition of (3) that will yield a given electrical output power P [W]. To do this, the Poisson's equation is initially solved with an arbitrary nonzero boundary condition $V = V_0^*$ at $\partial\Omega_{El2}$. Then, E^* and J^* are obtained from the solution and the corresponding electrical power P^* can be computed as $P^* = \int_\Omega E^* \cdot J^* d\mathbf{x}$. Since the solution and all the components of E and J are proportional to the value of V_0 we can scale the obtained solution, instead of recomputing it, in the following way:

$$V_0 = \lambda V_0^*, \quad E = \lambda E^*, \quad J = \lambda J^*, \quad \text{where} \quad \lambda = \sqrt{P/P^*}.$$

Let us note that this adjustment is performed only once at the beginning of the simulation. The obtained potential V_0 remains constant during the procedure.

For the numerical solution of problems (1)–(2) and (3)–(4) the finite element method in space is used [4]. We use *linear conforming tetrahedral finite elements*. Our unstructured grid parallel solver [7] is adapted for this problem. The element matrices are directly defined on the tetrahedrons of the used unstructured mesh (see Fig. 2). The meshing is done with the Netgen mesher [8]. An *algebraic multigrid* (AMG) preconditioner is used [3] in the PCG solution of the arising linear systems. The PCG and multigrid implementation from the Hypre library [2] are used. The time derivative can be discretized via finite differences and both the *backward Euler* and the *Crank-Nicolson* schemes can be used [5]. Let the matrices K and M be the stiffness and mass matrices from the finite element discretization of (1):

$$K = \left[\int_\Omega k\nabla\Phi_i \cdot \nabla\Phi_j d\mathbf{x}\right]_{i,j=1}^{N}, \qquad M = \left[\int_\Omega \rho c\Phi_i\Phi_j d\mathbf{x}\right]_{i,j=1}^{N}.$$

The electric field intensity is given by:

$$\mathbf{F} = \left[\int_\Omega J \cdot E\Phi_i d\mathbf{x}\right]_{i=1}^{N}, \tag{5}$$

Then, the spatially discretized parabolic equation (1) can be written in matrix form as:

$$M\frac{\partial \mathbf{T}}{\partial t} + K\mathbf{T} = \mathbf{F}. \tag{6}$$

The time discretization for both backward Euler method and the Crank-Nicolson one can be written in the form

$$(M + \tau^n \theta K)\,\mathbf{T}^{n+1} = (M - \tau^n (1-\theta) K)\,\mathbf{T}^n + \tau^n \mathbf{F}, \tag{7}$$

where the current (n-th) time-step is denoted with τ^n, the unknown solution at the next time step – with $\mathbf{T}^{n+1}$, and the solution at the current time step – with $\mathbf{T}^n$. If we set the parameter $\theta = 1$, (7) gives a system for the backward Euler discretization. When $\theta = 0.5$ (7) becomes Crank-Nicolson one.

3 Experiments

The material properties of the skin are taken from [9, 10]. The tick material properties are chosen to be close to the ones of the skin. All material properties used in the experiments are collected in Table 1. The entire domain is a cylinder with diameter 100 mm and height 100 mm. The thickness of the air layer is 50 mm, the one of the gel layer—0.1mm, all layers of the skin—49.9 mm. The thickness of epidermis is 0.5 mm. The dermis is 2 mm thick. The rest of the tissue is considered subcutis.

In all experiments the applied power P is set to 0.5W. Four different geometries with varying diameter of the electrodes $\varnothing$ and distance between them l are studied: $\varnothing = 1.5$ mm, $l = 5$ mm for Geometry 1; $\varnothing = 1.0$ mm, $l = 5$ mm for Geometry 2; $\varnothing = 1.5$ mm, $l = 7$ mm for Geometry 3 and $\varnothing = 1.0$ mm, $l = 7$ mm for Geometry 4. The meshes obtained from Netgen are refined uniformly by dividing each tetrahedron into 8 smaller ones. This refinement process is performed twice. We shall refer to the three different levels of refinement as *coarse, medium, and fine*. The backward Euler method is used in all numerical experiments. In the first set of experiments we are interested in numerical accuracy and stability of the discretization of the problem. We performed experiments on Geometry 2.

Table 1. Thermal and Electrical Properties of the Materials

Material	ρ (kg/m^3)	c (J/kg K)	k (W/m K)	σ (S/m)
Stainless steel	21 500	132	71	4×10^8
Gel	1 060	3 473.55	0.512	16
Epidermis	1 050	3 473.55	0.419	0.1
Dermis	1 050	3 473.55	0.314	0.6
Subcutis	1 050	3 473.55	0.209	0.6
Air	1	1	0.025	10^{-3}
Tick's body	1 050	3 473.55	0.512	1
Tick's mouth	1 050	3 473.55	0.512	0.6

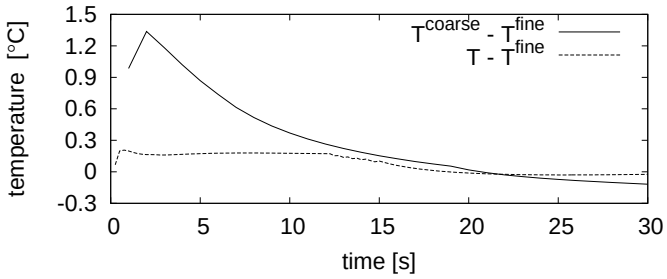

Fig. 3. Average temperature at tick's mouth, Geometry 2, compared to the ones on the finest mesh.

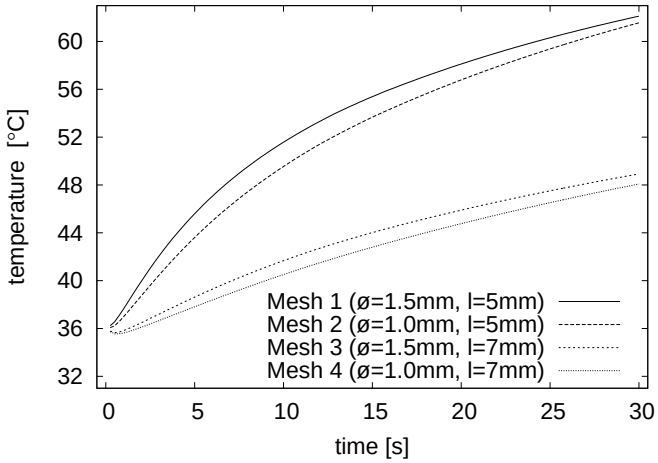

Fig. 4. Average temperature at tick's mouth, for different meshes.

On the coarse mesh time-step $\tau = 1$ is used, on the medium mesh – $\tau = 0.25$, and on the fine mesh – $\tau = 0.0625$. On Fig. 3, the averaged temperatures at tick's mouth T^{coarse} for the coarse mesh, T for the medium mesh, and T^{fine} for the fine mesh are compared. As we can see, there is no significant difference between the two finer meshes. Therefore, for the rest of the experiments we use a time-step of 0.25 and the medium meshes. Then we performed experiments with all four geometries. The averaged temperatures at tick's mouth are depicted on Fig. 4. Two cross-sections for the experiments on each mesh are presented on Fig. 5. There, isolines connect points with temperatures T=40°C, T=45°C, and T=50°C.

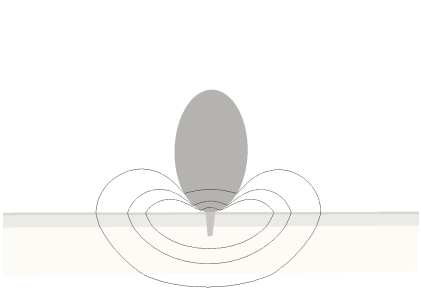

Geometry 1 YZ

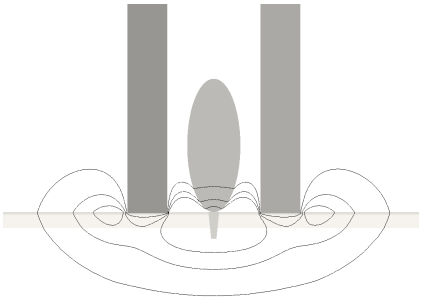

Geometry 1 XZ

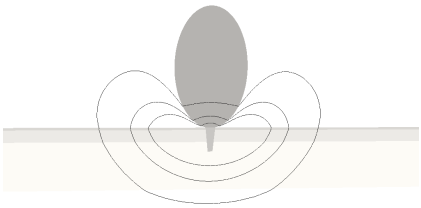

Geometry 2 YZ

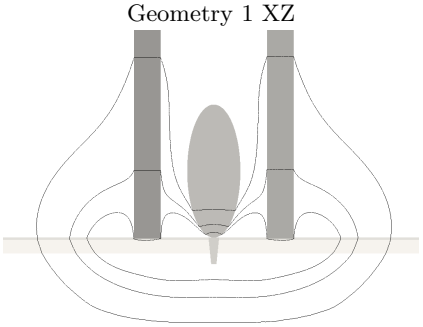

Geometry 2 XZ

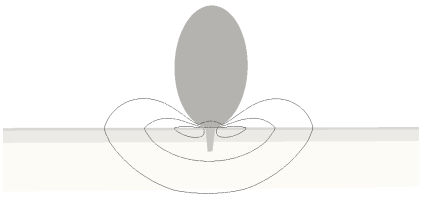

Geometry 3 YZ

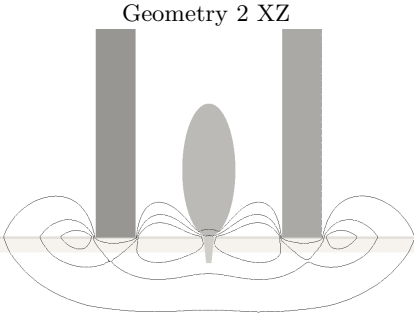

Geometry 3 XZ

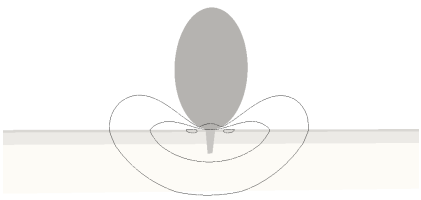

Geometry 4 YZ

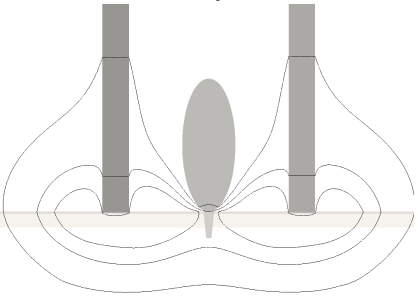

Geometry 4 XZ

Fig. 5. Isolines of the temperature: T=40°C, T=45°C, T=50°C at time t=30s

4 Discussion and Concluding Remarks

It is readily seen from the performed experiments that the results vary strongly depending on the distance between the electrodes. The thicker electrodes also produce more heat but this effect becomes less significant with time. This leads to the conclusion that the distance between electrodes in the actual apparatus should be carefully designed. Nevertheless in all four geometries, the temperature around tick's mouth is above 45°C. The applied power and/or procedure time can also be decreased.

It is important to note that our solver is general and can handle any unstructured tetrahedral mesh. Moreover it is parallelized using MPI and can handle big meshes – the finest mesh in these experiments has $\approx$ 144 million tetrahedrons.

Acknowledgment

This work is partially supported by the project AComIn „Advanced Computing for Innovation", grant 316087, funded by the FP7 Capacity Program. The collaboration with the development team from AMET Ltd is also acknowledged.

References

1. I. A. Chang and U. D. Nguyen *Thermal modeling of lesion growth with radiofrequency ablation devices* BioMedical Engineering OnLine 2004, 3:27
2. Lawrence Livermore National Laboratory Scalable Linear Solvers Project: `http://www.llnl.gov/CASC/linear_solvers/`.
3. Henson, V., Yang, U.: BoomerAMG: A parallel algebraic multigrid solver and preconditioner. Applied Numerical Mathematics 41(1), 155–177, Elsevier (2002)
4. Brenner, S., Scott, L.: The mathematical theory of finite element methods. Texts in applied mathematics 15, Springer-Verlag (1994)
5. Iserles, A.: A first course in the numerical analysis of differential equations. Cambridge University Press (2009)
6. Kosturski, N., Margenov, S., Vutov, Y.: Supercomputer Simulation of Radio-Frequency Hepatic Tumor Ablation. AMiTaNS'12 Proceedings, AIP CP 1487, 120–126 (2012)
7. Georgiev, K., Kosturski, N., Vutov, Y.: On the Adaptive Time-Stepping in Radio-Frequency Liver Ablation Simulation: Some Preliminary Results, Large-Scale Scientific Computing, LNCS 8353, 397–404 (2014)
8. Schöberl, J.: *NETGEN An advancing front 2D/3D-mesh generator based on abstract rules*, Computing and Visualization in Science, 41–52, Springer-Verlag (1997)
9. Gurung, D.: Thermoregulation Through Skin at Low Atmospheric Temperatures. Kathmandu University Journal of Science, Engineering and Technology 5(I), 14–22 (2009)
10. Gabriel, C., Peyman, A., Grant, E.: Electrical conductivity of tissue at frequencies below 1 MHz, Phys. Med. Biol. 54(16), 4863–4878 (2009)
11. COMSOL, Inc.: COMSOL Multiphysics: AC/DC Module User's Guide. (2008)